Magnetic x-ray spectroscopy of Gd-doped EuO thin films

E. L. Arnold,[1,2] J. M. Riley,[2,3,*] L. B. Duffy,[1,†] A. I. Figueroa,[2,‡] R. Held,[4,§] K. M. Shen,[5,6] D. G. Schlom,[4,6,7] P. D. C. King,[3] M. Hoesch,[2,8] G. van der Laan,[2] and T. Hesjedal[1,2,‖]

[1]*Department of Physics, Clarendon Laboratory, University of Oxford, Oxford OX1 3PU, United Kingdom*
[2]*Diamond Light Source, Harwell Science and Innovation Campus, Didcot OX11 0DE, United Kingdom*
[3]*SUPA, School of Physics and Astronomy, University of St Andrews, St Andrews KY16 9SS, United Kingdom*
[4]*Department of Materials Science & Engineering, Cornell University, Ithaca, New York 14853, USA*
[5]*Department of Physics, Cornell University, Ithaca, New York 14853, USA*
[6]*Kavli Institute at Cornell for Nanoscale Science, Ithaca, New York 14853, USA*
[7]*Leibniz-Institut für Kristallzüchtung, Max-Born-Str. 2, 12489 Berlin, Germany*
[8]*DESY Photon Science, Notkestr. 85, D-22607 Hamburg, Germany*

(Received 8 November 2024; accepted 3 February 2025; published 24 February 2025)

We present a detailed x-ray magnetic circular dichroism (XMCD) study of the magnetic properties of Gd-doped EuO thin films, synthesized via molecular-beam epitaxy with Gd doping levels up to over 12%. The impact of Gd doping on the electronic and magnetic behavior of EuO is studied using XMCD and magnetometry. Gd doping significantly enhances the Curie temperature (T_C) from 69 K in undoped EuO to over 120 K, driven by increased carrier density, while preserving the high quality of the single-crystalline films. At higher doping levels, a plateau in T_C is observed, which is attributed to the formation of Eu-Gd nearest-neighbor pairs that limit dopant activation. We also observe a distinctive "double-dome" structure in the temperature-dependent magnetization, which we attribute to both the ferromagnetic ordering of Eu $4f$ moments at lower temperatures and the influence of conduction electrons via $4f$-$5d$ exchange interactions at higher temperatures. These findings provide key insights into the mechanisms of carrier-induced magnetic transitions.

DOI: 10.1103/PhysRevMaterials.9.024410

I. INTRODUCTION

The transport, control, and read-out of spin currents underpins the design of spintronic devices. Owing to the strong reduction of the spin current in semiconductor-metal interfaces, magnetic semiconductors have been explored as candidate spintronic device materials. Eu(II) monoxide (EuO) is a rare example of a ferromagnetic oxide semiconductor [1]. It is known to host a wide range of phenomena, including a large metal-insulator transition of up to 13 orders of magnitude [2], a colossal magnetoresistance up to 6 orders of magnitude [3], the giant magneto-optic Kerr [4] and Faraday [5,6] effects, and the anomalous Hall effect [7].

Unfortunately, stoichiometric EuO is problematic for its use in devices, due to its low Curie temperature of 69 K [8]. Tuning the Curie temperature to higher values through doping is one possible route toward EuO-based devices. Doping EuO with trivalent elements, or alternatively by introducing oxygen deficiency [9], is known to increase the Curie temperature up to 129 K [10].

EuO thin films have been grown on a wide range of substrates, including Si [11], GaAs [12], GaN [9], and graphene [13], making it, in principle, an ideal candidate for emerging spintronic technology incorporated with current semiconductor production processes. Nevertheless, preserving a pristine interface in Si/EuO heterostructures has proved challenging. On the other hand, oxide substrates such as yttria-stabilized cubic zirconia (YSZ) [13], $LaAlO_3$ [14], and $YAlO_3$ [15] readily allow sharp interfaces with stoichiometric EuO, provided precautions are taken to avoid overoxidation. Note that YSZ releases oxygen into the initial layers of the deposited film [13].

Here, we study the properties of Gd-doped EuO using x-ray magnetic circular dichroism (XMCD) in conjunction with superconducting quantum interference device (SQUID) magnetometry, exploring the peculiar interplay between EuO's magnetic and electrical properties. Following previous studies [9,10,16–20], we link the enhancement in the Curie temperature to the increase in carrier density, using temperature-dependent XMCD to demonstrate how the Eu and Gd sublattice moments evolve through the transition.

*Current address: Perbak Capital, Park Drive, Milton Park, Oxford OX14 4SB, United Kingdom.
†Current address: Haileybury School, Hertford, SG13 7NU, United Kingdom.
‡Current address: Departament de Física de la Matèria Condensada and IN2UB, Universitat de Barcelona, ES-08028 Barcelona, Spain.
§Current address: Deutsches Patent- und Markenamt, D-80331 München, Germany.
‖Contact author: thorsten.hesjedal@physics.ox.ac.uk

II. SAMPLE PREPARATION AND ELECTRONIC PROPERTIES

EuO exhibits unique magnetic and electronic properties but is unstable in air, oxidizing quickly to Eu_3O_4 and Eu_2O_3, which lack the same characteristics. This necessitates careful *in situ* growth and measurement. Single-crystalline Gd-doped EuO films were grown using molecular-beam epitaxy (MBE) on $YAlO_3$ substrates, utilizing the miniMBE system installed on the I05 beamline at the Diamond Light Source (Oxfordshire, UK) [21]. The high-quality samples used here have been well characterized during a previous study [18]. During growth, precise control of O_2 and Eu fluxes, substrate temperature (425°C), and dopant introduction ensured stoichiometric EuO growth while minimizing oxygen vacancies and higher oxidation states [13,15]. The films were analyzed in real time using reflection high-energy electron diffraction (RHEED), showing smooth transitions indicative of high crystal quality. Adjustments to the Gd flux and careful monitoring of the RHEED patterns demonstrated that optimal doping preserves film homogeneity, while overdoping causes structural inhomogeneities.

After growth, the films were transferred under ultrahigh vacuum for angle-resolved photoemission spectroscopy (ARPES), x-ray photoelectron spectroscopy (XPS), and low-energy electron diffraction characterization, confirming the structural and chemical properties. The carrier densities of the doped films were determined from ARPES measurements by extracting the Luttinger volume from the measured Fermi surfaces in conjunction with simulations as discussed in detail in Ref. [18]. To protect these air-sensitive samples, they were capped with a thin layer of amorphous silicon at room temperature to limit oxidation during further measurements.

III. MAGNETIC X-RAY SPECTROSCOPY

XMCD is an element-specific technique used to probe the local electronic character of the magnetic ground state [22]. X-ray absorption spectra (XAS) at the Eu and Gd $M_{4,5}$ edges ($3d \rightarrow 4f$) of Gd-doped EuO thin films were measured from 60 to 150 K using the 14 T superconducting magnet on beamline I10 at Diamond. The degree of circular polarization of the x-ray beam in the energy region of interest is close to 100%. XAS measurements were made in the total-electron yield (TEY) mode, which is surface sensitive with an exponentially decreasing probing depth of ∼6 nm [23]. The XMCD is obtained from the difference between two XAS spectra recorded with the x-ray helicity vector antiparallel and parallel to the applied magnetic field.

Experimental XMCD spectra and their theoretical counterparts for the 12.2%-doped sample at 50 K are shown in Fig. 1 and Fig. S1 in the Supplemental Material [24]. The M_5 peak maximum for Eu_2O_3 is at ∼2.5 eV higher photon energy than that of EuO [23,25,26]. Its absence means that the amount of Eu^{3+} in our samples is very small, consistent with our XPS measurements shown in Ref. [18]. Figure 1 shows an excellent agreement between experimental and theoretical XMCD spectra. The good spectral agreement for the rare-earth $M_{4,5}$ edge is primarily due to the localized nature of the $4f$ electrons [23,27–29]. Eu and Gd share the same $4f^7$ ground state, and therefore display very similar XAS and XMCD multiplet structures, aside from differences in line width and photon energy [23]. The photon energies of the M_5 peak maxima were calibrated to 1128.1 eV for Eu^{2+} and 1184.1 eV for Gd^{3+} [23].

In our calculations of the theoretical XAS and XMCD spectra, the intrinsic lifetime broadening is taken as a Lorentzian with a half-width at half-maximum of $\Gamma = 0.4\,(0.5)$ eV for the M_5 (M_4) edge for both Eu and Gd. The instrumental broadening is included as a Gaussian with standard deviation $\sigma = 0.6\,(0.4)$ eV for Eu (Gd). While the Gd $M_{4,5}$ shows a similar Gaussian broadening as previously observed for Gd containing materials [23,30], the broadening for the Eu $M_{4,5}$ is larger than in some other reports [23,31] but similar to that of other EuO films reported in the literature [16,25].

Electric-dipole transitions from the $3d$ core level are allowed to empty $4f$ states but forbidden to $5d$ and $6s$ valence states. For the multielectronic configuration of the Eu^{2+} and Gd^{3+} ions, the transitions $4f^7 \rightarrow 3d^9 4f^8$ are calculated using atomic multiplet theory, in which spin-orbit and electrostatic interactions are treated on an equal footing [23,27]. The $4f$ wave function contraction in the lanthanide series renders these orbitals atomic-like, with negligible influence on the local environment. The localized character of the $4f$ state is confirmed by the small reduction factor of the Slater integrals and by the fact that crystal-field interactions only play a negligible role in the calculation. The parameters of the Slater integrals for the Coulomb and exchange interactions were reduced to 80% and 84% for Eu and Gd, respectively [23]. The intraatomic electrostatic interactions include the $3d$-$4f$ and $4f$-$4f$ Coulomb and exchange interactions. The wave functions of the initial- and final-state configurations are calculated in intermediate coupling using Hartree-Fock theory with relativistic corrections [32,33].

In principle, the magnitude of the XMCD signal is proportional to the $4f$ magnetic moment. One could employ the celebrated sum-rule analysis [34–36], as is customary for $3d$ transition metals. While for light rare earths (Ce to Sm) the strong jj mixing between the $3d_{5/2}$ and $3d_{3/2}$ core levels requires a large correction factor in the sum-rule analysis [42], for Eu^{2+} and Gd^{3+} f^7 this correction factor is 0.949 (which means a 5% correction). Also, the magnetic dipole term, appearing as an additional contribution to the spin sum rule, is (close to) zero. However, other errors play a more important role in the accuracy of the sum rules. Figures 1(c) and 1(d) show that there is a drift in the background signal. While this is not a real problem for obtaining the relative intensity of a given peak, it becomes problematic when taking the integrated intensity over a broad energy range. A small offset can lead to a large error in the integral. Therefore, it turned out that taking the asymmetry A is a much more reliable method to obtain relative spin moments (the orbital moment is about zero for f^7).

As an alternative to the sum rule method, the results were analyzed using the peak asymmetry A, i.e., for a given absorption edge, the XMCD peak amplitude divided by the sum of the XAS peak amplitudes. From the calculations using the data in Fig. 1, for the Eu $4f^7$ spectra we obtain $A = 0.497$ for the Hund's rule ground state, which has an effective moment $\mu_{\text{eff}} = 7.93\,\mu_B$ per atom. For the Gd $4f^7$ spectra, with their

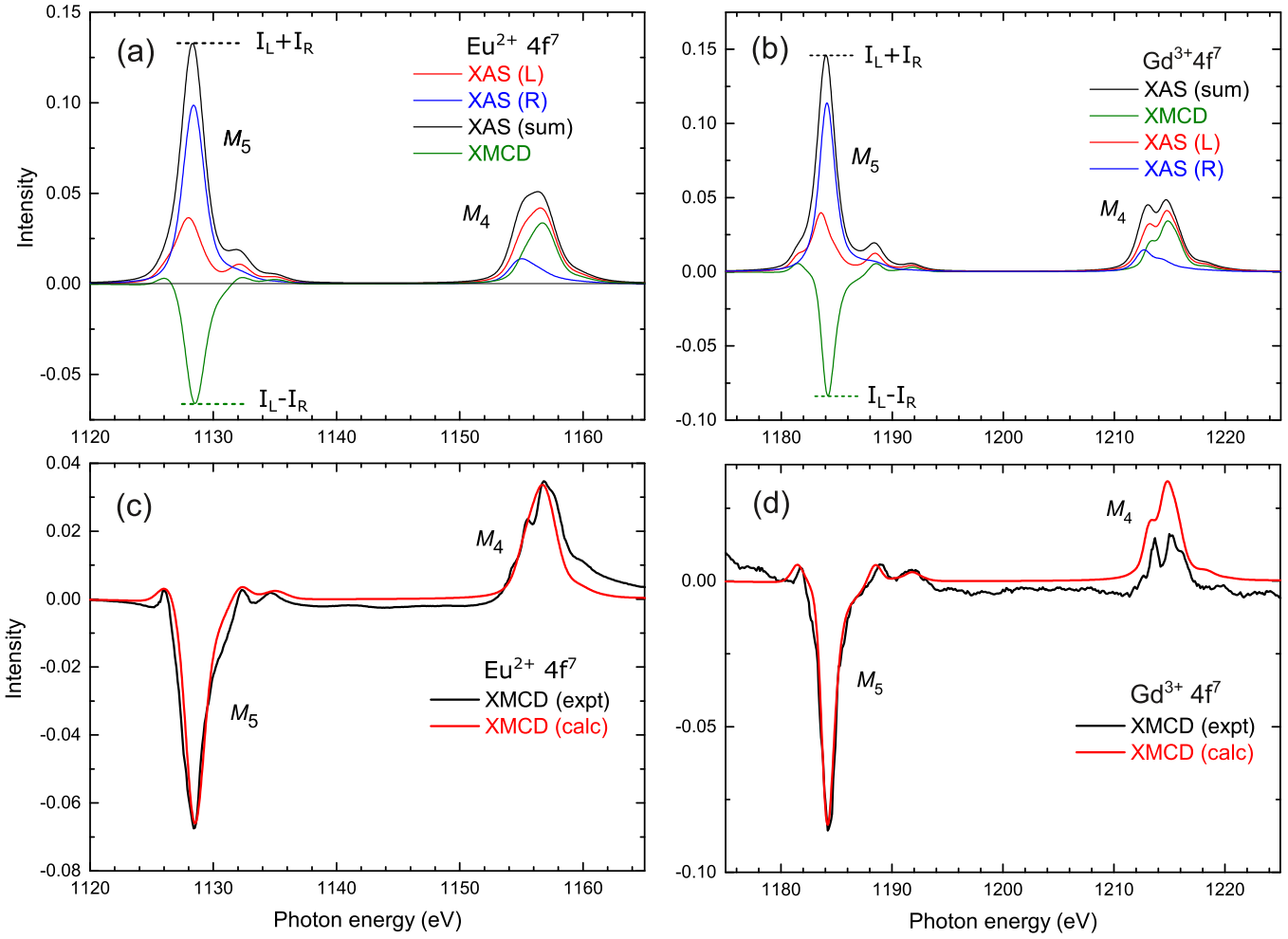

FIG. 1. Eu^{2+} and Gd^{3+} $M_{4,5}$ XAS and XMCD spectra for the 12.2%-doped sample at 50 K. (a), (b) Calculated XAS for left- and right-circular polarization together with the sum and difference (i.e., XMCD) spectrum for Eu^{2+} and Gd^{3+}, respectively. The asymmetry A, defined as the maximum of the XMCD divided by the corresponding sum signal, $(I_L - I_R)/(I_L + I_R)$, is 0.497 and 0.5896 for the Hund's rule ground-state value of the magnetic moment for Eu and Gd, respectively. See Supplemental Material [24] for a worked-out example calculation for this sample. (c), (d) Comparison of calculated and experimental Eu and Gd XMCD for Gd-doped EuO. All XMCD spectra were measured in TEY mode at remanence (∼30 mT) in the superconducting magnet (i.e., above the coercive field; see Fig. 2).

narrower line broadening, $A = 0.5896$, also corresponding to $\mu_{\text{eff}} = 7.93\,\mu_B$ per atom. The proportionality between A and the magnetic moment per atom allows the magnetic moment per atom to be determined [30,37]. An example of a calculation is discussed in the Supplemental Material [24].

Next, we investigated the temperature-dependent contributions of both Eu and Gd to the magnetic behavior of Gd-doped EuO for three temperatures below the T_C (∼120 K) of a 7.1%-doped sample. As shown in Fig. 2(a), at the Eu M_5 edge, the hysteresis loop displays a clear ferromagnetic behavior at 80 K, with a large loop opening. The asymmetry diminishes with increasing temperature toward T_C, as well as the coercive field, suggesting that the Eu-based magnetic order is closely aligned with the film's overall Curie temperature. In contrast, for the hysteresis loops measured at the Gd M_5 edge [Fig. 2(b)], the magnetic response of the Gd ions has almost vanished at 120 K, while the decrease of the asymmetry going from 80 to 100 K is less pronounced. Thus, while at lower temperatures the gradual reduction in asymmetry with temperature implies that the Gd^{3+}-driven magnetization is coupled to the Eu^{2+} subsystem, at 120 K close to T_C, Gd itself does not appear to be magnetically ordered. This behavior hints at the electronic contributions of Gd ions to the stabilization of magnetic order.

The temperature evolution of the net magnetic moments of our Gd-doped EuO samples, obtained using SQUID magnetometry (measured in an applied field of 200 Oe after zero-field cooling [18]), is plotted in Fig. 3(a), with the temperature derivative of the magnetometry data plotted in Fig. 3(b). The line shapes show qualitative agreement with the trend established by Mairoser *et al.* for measurements in low applied magnetic fields [38]. Alongside these data, Fig. 3(c) shows the XMCD magnetization measurements (measured at remanence in the superconducting magnet) normalized to the SQUID magnetometry data, enabling a direct comparison of the Eu and Gd moments.

We estimated the Curie temperature using two methods: (1) by extracting the positions of the peaks in dM/dT

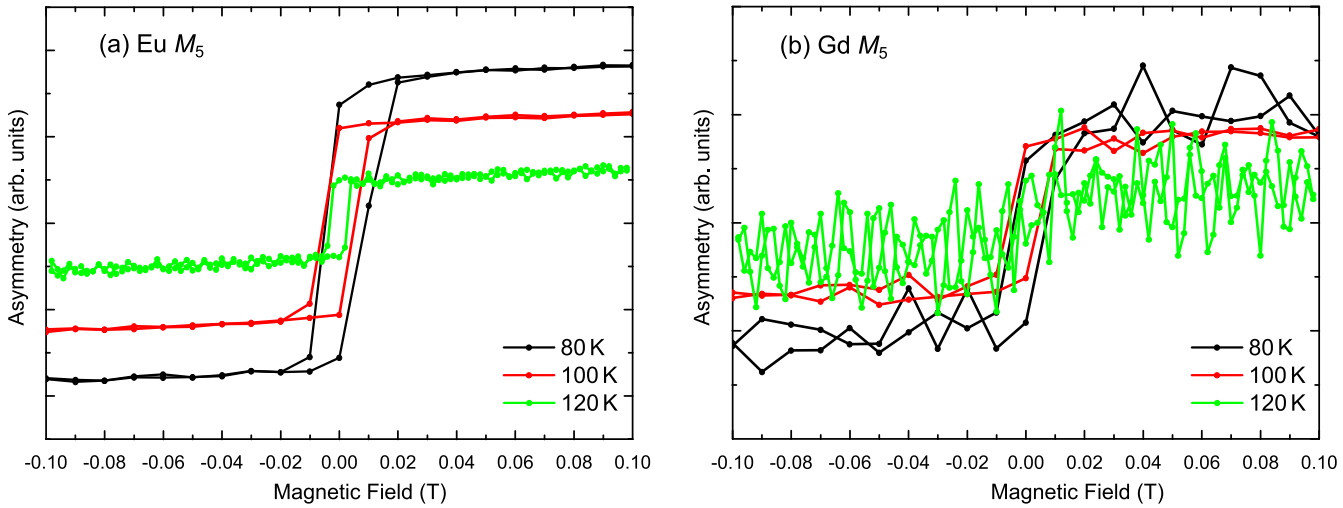

FIG. 2. XMCD hysteresis loops measured at (a) the Eu M_5 and (b) Gd M_5 edges for a 7.1% Gd-doped sample at 80, 100, and 120 K. The asymmetry is shown in arbitrary units. The loops were taken with the x-ray beam at 30° to the sample normal.

measured using SQUID magnetometry, and (2) by identifying the temperature above which the characteristic XMCD line shape for ferromagnetically ordered species starts to break down. To demonstrate the carrier-activated enhancement of T_C [39], the carrier concentration is plotted alongside the extracted Curie temperatures as a function of Gd doping in Fig. 3(d). Here, the nominal Gd doping percentage is determined by taking the ratio of Eu to Gd M_5 XAS peak amplitudes. It can be seen that, for sufficiently high Gd doping, the carrier density becomes strongly correlated with T_C. Although previous studies have demonstrated the strong connection between n and T_C, here we have confirmed that (1) the

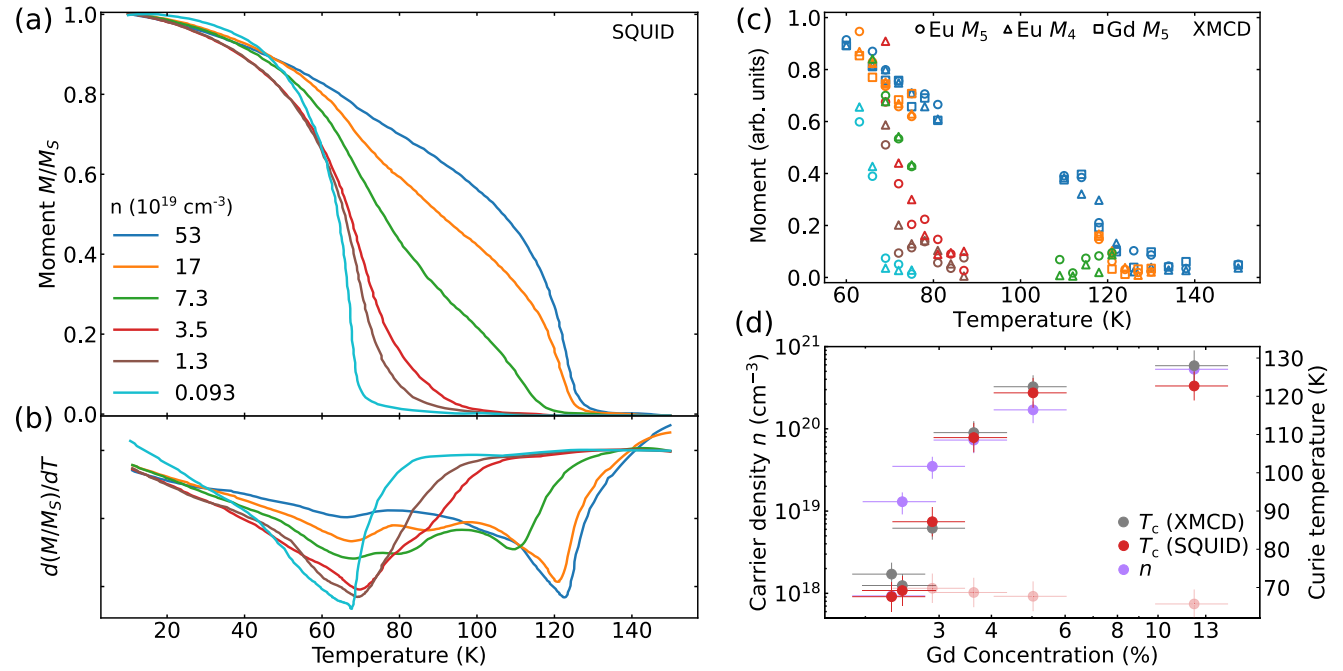

FIG. 3. Temperature-dependent magnetic properties of Gd-doped EuO. (a) Normalized magnetic moments for various carrier densities n measured with SQUID magnetometry. (b) Derivative of the SQUID $M(T)$. The shift in the peaks from ∼69 K to >90 K indicate a carrier-induced enhancement of T_C. (c) XMCD asymmetry (in arbitrary units, with the XMCD moments normalized to the SQUID magnetometry data) obtained for each absorption edge, for each sample (except for very low Gd doping levels, for which the XMCD signal was too weak), over a wide temperature range. The circles denote Eu M_5 data, triangles denote Eu M_4 data, and squares denote Gd M_5 data. The measurements were made at remanence in the superconducting magnet. The element specificity of XMCD indicates that the Eu moments and Gd moments have comparable line shapes throughout the studied temperature range. The color schemes of (b) and (c) follow that of (a). (d) Effect of Gd concentration on the Curie temperature, obtained through SQUID (red dots) and XMCD (gray dots), and the carrier density (purple dots), measured with ARPES (see Ref. [18]). The transparent red dots indicate the position of the diminishing peak in dM/dT near 69 K.

peaks in dM/dT correspond to magnetic phase transitions, corroborated with the onset of XMCD, and (2), with evidence from both XMCD and magnetometry compared to ARPES [18], that a sufficiently high doping level is required for n and T_C to become harmonized. This coincides with the increasing suppression of the peak in dM/dT near 69 K.

IV. DISCUSSION

The dM/dT curves reveal that the increase in doping induces the peak near 69 K (the Curie temperature of undoped EuO) to become broader and less intense, as well as to shift to higher temperatures, indicative of an enhancement of T_C. Due to the relatively sparse distribution of Gd atoms in this doping regime, there are two kinds of Eu-Gd configurations plausible in the crystal lattice: (1) an Eu atom with one Gd nearest neighbor (NN), i.e., ignoring the O atoms which do not contribute to the magnetic ordering, and (2) an Eu atom that is isolated from Gd sites. The former of these will contribute to domains with slightly higher T_C, which manifests itself as an elongated tail in the $M(T)$ curves.

Increasing the Gd concentration enhances the abundance of Eu-Gd NN configurations, thereby potentially being the cause of the second peak in dM/dT at higher temperatures. While the presence of peaks in dM/dT at both 69 K and >90 K could potentially be attributed to an inhomogeneous dopant distribution [40], where there are regions of doped and undoped EuO, here such configurations are the result of dilute doping. For sufficiently high Gd, almost all Eu sites have at least one Gd NN, leading to the near disappearance of the peak at 69 K.

At sufficiently high doping levels, the strong correlation between T_C and n is clear in Fig. 3(d). The plateau observed in both T_C and n at higher Gd concentrations is not solely due to saturation of Eu-Gd NN sites, but rather to a reduction in dopant activation efficiency. As more Gd atoms form multiple NN pairs, carrier activation diminishes at elevated temperatures, likely due to clustering effects, as noted in Ref. [39].

This double-dome structure in the temperature-dependent magnetization $M(T)$ of Gd-doped EuO has been observed in several experimental studies on EuO [38,41], as well as in theoretical work [42,43]. It arises from two distinct magnetic ordering phenomena, each associated with different interactions and subsystems within the material. The first dome corresponds to the magnetic ordering of the Eu^{2+} ions, which are responsible for the intrinsic ferromagnetism in undoped EuO [1]. In pure EuO, this ordering typically occurs at its T_C of $\sim$69 K [44]. In Gd-doped EuO, the magnetic moments of the Eu^{2+} ions still dominate the magnetic behavior at lower temperatures.

The ferromagnetism of the Eu subsystem originates from the indirect Heisenberg exchange interaction, which is mediated through the oxygen atoms. This interaction aligns the spins of the Eu^{2+} ions, leading to a ferromagnetic phase with a specific transition temperature [45]. When Gd is doped into EuO, the Curie temperature associated with the Eu subsystem typically shifts to slightly higher temperatures (but remains lower than for the second dome) due to the modification of exchange interactions by the conduction electrons introduced by Gd [10,46]. The first dome represents this ferromagnetic transition, associated primarily with the Eu spins.

The second dome arises from the magnetic ordering involving both the Eu^{2+} and Gd^{3+} ions, but it is primarily driven by the interaction of the conduction electrons introduced by the Gd doping [46]. Gd ions contribute itinerant electrons to the conduction band, which enhances the magnetic coupling between the Eu ions through a carrier-mediated interaction [10]. The conduction electrons donated by Gd facilitate a Ruderman-Kittel-Kasuya-Yosida (RKKY) interaction between the localized Eu moments [46]. This interaction is mediated by the spin polarization of the conduction electrons, which couple the localized spins of Eu and Gd in a long-range ferromagnetic manner [17]. The second dome occurs at a higher temperature than the first dome, reflecting the fact that the Gd-induced conduction electrons strengthen the ferromagnetic coupling beyond the intrinsic $Eu^{2+} - Eu^{2+}$ interaction. This second transition temperature can be significantly higher than the first, pushing the overall T_C of the system toward values as high as 150–200 K, depending on the Gd doping level [46].

The two domes reflect different energy scales: the first dome is related to the localized exchange interaction between Eu spins, while the second dome involves the longer-range coupling mediated by the conduction electrons, which interact with both Eu and Gd moments [46]. As the temperature increases, the system transitions from being dominated by the localized Eu^{2+} moments (first dome) to being dominated by the carrier-mediated interactions involving both Eu and Gd (second dome) [10]. The enhancement of T_C and double-dome character has also been linked to the presence of bound magnetic polarons [8,47,48].

V. CONCLUSIONS

In conclusion, we investigated the magnetic properties of Gd-doped EuO thin films synthesized using MBE. Through *in vacuo* transfers, a complementary set of data of the structural and electronic properties on the same set of samples was gained previously, as presented in Ref. [18]. Through XMCD-compatible capping with Si, we were able to carry out magnetic spectroscopy on pristine samples. In accordance with other studies, we find that Gd doping raises the T_C of EuO. We show that, at higher doping levels, T_C (measured with magnetometry and XMCD) and carrier density n become highly correlated. Toward these higher doping levels, a plateau in T_C is observed, which had been attributed to the formation of Eu-Gd nearest-neighbor pairs that limit dopant activation. Our XMCD measurements at the Eu and Gd $M_{4,5}$ edges reveal a robust $4f$ magnetic moment for Eu, consistent with a Hund's rule ground state with an effective moment of $\sim$7.93 μ_B/Eu atom. We were able to confirm a minimal Eu^{3+} content, corroborated by the absence of Eu_2O_3-like features. Further, in the temperature-dependent magnetization, we observed a distinctive double-dome behavior, linked to the ferromagnetic ordering of Eu $4f$ moments at lower temperatures and the influence of conduction electrons through $4f$-$5d$ exchange interactions at higher temperatures.

ACKNOWLEDGMENTS

Beamtime awarded on I05 (ARPES) and I10 (XMCD) at the Diamond Light Source, UK (Proposals No. SI16162 and No. NT15481) is acknowledged. P.D.K. further gratefully acknowledges support from the Royal Society (Grant No. UF120096) and the Leverhulme Trust (Grants No. PLP-2015-144 and No. RPG-2023-256). J.M.R. acknowledges the Engineering and Physical Sciences Research Council (EPSRC), UK, for PhD studentship support through Grant No. EP/L505079/1. L.B.D. acknowledges studentship support from EPSRC (Grant No. EP/G03673X/1) and the Science and Technology Facilities Council (UK), and E.L.A. from EPSRC (Grant No. EP/W524311/1) and the Diamond Light Source. The work at Cornell University was supported by the National Science Foundation (NSF) [Platform for the Accelerated Realization, Analysis, and Discovery of Interface Materials (PARADIM)] under Cooperative Agreement No. DMR-2039380.

[1] B. T. Matthias, R. M. Bozorth, and J. H. Van Vleck, Ferromagnetic interaction in EuO, Phys. Rev. Lett. **7**, 160 (1961).

[2] G. Petrich, S. von Molnár, and T. Penney, Exchange-induced autoionization in Eu-rich EuO, Phys. Rev. Lett. **26**, 885 (1971).

[3] Y. Shapira, S. Foner, and T. B. Reed, EuO. I. Resistivity and Hall effect in fields up to 150 kOe, Phys. Rev. B **8**, 2299 (1973).

[4] J. C. Suits and K. Lee, Giant magneto-optical Kerr effect in EuO, J. Appl. Phys. **42**, 3258 (1971).

[5] K. Y. Ahn and M. W. Shafer, Relationship between stoichiometry and properties of EuO films, J. Appl. Phys. **41**, 1260 (1970).

[6] C.-C. Huang and J. T. Ho, Faraday rotation near the Curie point of EuO, Phys. Rev. B **12**, 5255 (1975).

[7] T. Yamasaki, K. Ueno, A. Tsukazaki, T. Fukumura, and M. Kawasaki, Observation of anomalous Hall effect in EuO epitaxial thin films grown by a pulse laser deposition, Appl. Phys. Lett. **98**, 082116 (2011).

[8] A. Mauger and C. Godart, The magnetic, optical, and transport properties of representatives of a class of magnetic semiconductors: The europium chalcogenides, Phys. Rep. **141**, 51 (1986).

[9] A. Schmehl, V. Vaithyanathan, A. Herrnberger, S. Thiel, C. Richter, M. Liberati, T. Heeg, M. Röckerath, L. F. Kourkoutis, S. Mühlbauer, P. Böni, D. A. Muller, Y. Barash, J. Schubert, Y. Idzerda, J. Mannhart, and D. G. Schlom, Epitaxial integration of the highly spin-polarized ferromagnetic semiconductor EuO with silicon and GaN, Nat. Mater. **6**, 882 (2007).

[10] T. Mairoser, A. Schmehl, A. Melville, T. Heeg, L. Canella, P. Böni, W. Zander, J. Schubert, D. E. Shai, E. J. Monkman, K. M. Shen, D. G. Schlom, and J. Mannhart, Is there an intrinsic limit to the charge-carrier-induced increase of the Curie temperature of EuO? Phys. Rev. Lett. **105**, 257206 (2010).

[11] J. Lettieri, V. Vaithyanathan, S. K. Eah, J. Stephens, V. Sih, D. D. Awschalom, J. Levy, and D. G. Schlom, Epitaxial growth and magnetic properties of EuO on (001) Si by molecular-beam epitaxy, Appl. Phys. Lett. **83**, 975 (2003).

[12] A. G. Swartz, J. Ciraldo, J. J. I. Wong, Y. Li, W. Han, T. Lin, S. Mack, J. Shi, D. D. Awschalom, and R. K. Kawakami, Epitaxial EuO thin films on GaAs, Appl. Phys. Lett. **97**, 112509 (2010).

[13] R. Sutarto, S. G. Altendorf, B. Coloru, M. Moretti Sala, T. Haupricht, C. F. Chang, Z. Hu, C. Schüßler-Langeheine, N. Hollmann, H. Kierspel, H. H. Hsieh, H.-J. Lin, C. T. Chen, and L. H. Tjeng, Epitaxial and layer-by-layer growth of EuO thin films on yttria-stabilized cubic zirconia (001) using MBE distillation, Phys. Rev. B **79**, 205318 (2009).

[14] C. Caspers, Magnetic Oxide Heterostructures: EuO on Cubic Oxides and on Silicon, Ph.D. thesis, Universität Duisburg-Essen, 2013.

[15] R. W. Ulbricht, A. Schmehl, T. Heeg, J. Schubert, and D. G. Schlom, Adsorption-controlled growth of EuO by molecular-beam epitaxy, Appl. Phys. Lett. **93**, 102105 (2008).

[16] H. Ott, S. J. Heise, R. Sutarto, Z. Hu, C. F. Chang, H. H. Hsieh, H.-J. Lin, C. T. Chen, and L. H. Tjeng, Soft x-ray magnetic circular dichroism study on Gd-doped EuO thin films, Phys. Rev. B **73**, 094407 (2006).

[17] N. Jutong, U. Eckern, T. Mairoser, and U. Schwingenschlögl, Effect of Gd doping and O deficiency on the Curie temperature of EuO, Sci. Rep. **5**, 8038 (2015).

[18] J. M. Riley, F. Caruso, C. Verdi, L. B. Duffy, M. D. Watson, L. Bawden, K. Volckaert, G. van der Laan, T. Hesjedal, M. Hoesch, F. Giustino, and P. D. C. King, Crossover from lattice to plasmonic polarons of a spin-polarised electron gas in ferromagnetic EuO, Nat. Commun. **9**, 2305 (2018).

[19] R. Held, T. Mairoser, A. Melville, J. A. Mundy, M. E. Holtz, D. Hodash, Z. Wang, J. T. Heron, S. T. Dacek, B. Holländer, D. A. Muller, and D. G. Schlom, Exploring the intrinsic limit of the charge-carrier-induced increase of the curie temperature of Lu- and La-doped EuO thin films, Phys. Rev. Mater. **4**, 104412 (2020).

[20] V. Goian, R. Held, E. Bousquet, Y. Yuan, A. Melville, H. Zhou, V. Gopalan, P. Ghosez, N. A. Spaldin, D. G. Schlom, and S. Kamba, Making EuO multiferroic by epitaxial strain engineering, Commun. Mater. **1**, 74 (2020).

[21] A. A. Baker, W. Braun, G. Gassler, S. Rembold, A. Fischer, and T. Hesjedal, An ultra-compact, high-throughput molecular beam epitaxy growth system, Rev. Sci. Instrum. **86**, 043901 (2015).

[22] G. van der Laan and A. I. Figueroa, X-ray magnetic circular dichroism—Aversatile tool to study magnetism, Coord. Chem. Rev. **277-278**, 95 (2014).

[23] B. T. Thole, G. van der Laan, J. C. Fuggle, G. A. Sawatzky, R. C. Karnatak, and J. M. Esteva, $3d$ x-ray-absorption lines and the $3d^9 4f^{n+1}$ multiplets of the lanthanides, Phys. Rev. B **32**, 5107 (1985).

[24] See Supplemental Material at http://link.aps.org/supplemental/10.1103/PhysRevMaterials.9.024410 for the determination of the spin moment from the XMCD asymmetry.

[25] E. Negusse, J. Holroyd, M. Liberati, J. Dvorak, Y. U. Idzerda, T. S. Santos, J. S. Moodera, and E. Arenholz, Effect of electrode and EuO thickness on EuO-electrode interface in tunneling spin filter, J. Appl. Phys. **99**, 08E507 (2006).

[26] V. Kachkanov, M. J. Wallace, G. van der Laan, S. S. Dhesi, S. A. Cavill, Y. Fujiwara, and K. P. O'Donell, Induced magnetic moment of Eu^{3+} ions in GaN, Sci. Rep. **2**, 969 (2012).

[27] G. van der Laan, Hitchhiker's guide to multiplet calculations, Lect. Notes Phys. **697**, 143 (2006).

[28] G. van der Laan, B. T. Thole, G. A. Sawatzky, J. B. Goedkoop, J. C. Fuggle, J. M. Esteva, R. C. Karnatak, J. P. Remeika, and H. A. Dabkowska, Experimental proof of magnetic x-ray dichroism, Phys. Rev. B **34**, 6529 (1986).

[29] G. van der Laan, E. Arenholz, Z. Hu, A. Bauer, E. Weschke, C. Schüssler-Langeheine, E. Navas, A. Mühlig, G. Kaindl, J. B. Goedkoop, and N. B. Brookes, Magnetic circular dichroism in Tb $3d \rightarrow 4f$ resonant photoemission, Phys. Rev. B **59**, 8835 (1999).

[30] S. E. Harrison, L. J. Collins-McIntyre, S. Li, A. A. Baker, L. R. Shelford, Y. Huo, A. Pushp, S. S. P. Parkin, J. S. Harris, E. Arenholz, G. van der Laan, and T. Hesjedal, Study of Gd-doped Bi_2Te_3 thin films: Molecular beam epitaxy growth and magnetic properties, J. Appl. Phys. **115**, 023904 (2014).

[31] G. van der Laan, E. Arenholz, A. Schmehl, and D. G. Schlom, Weak anisotropic x-ray magnetic linear dichroism at the Eu $M_{4,5}$ edges of ferromagnetic EuO(001): Evidence for $4f$-state contributions, Phys. Rev. Lett. **100**, 067403 (2008).

[32] R. D. Cowan, *The Theory of Atomic Structure and Spectra* (University of California, Berkeley, 1992).

[33] G. van der Laan and B. T. Thole, Strong magnetic x-ray dichroism in $2p$ absorption spectra of $3d$ transition-metal ions, Phys. Rev. B **43**, 13401 (1991).

[34] B. T. Thole, P. Carra, F. Sette, and G. van der Laan, X-ray circular dichroism as a probe of orbital magnetization, Phys. Rev. Lett. **68**, 1943 (1992).

[35] P. Carra, B. T. Thole, M. Altarelli, and X. Wang, X-ray circular dichroism and local magnetic fields, Phys. Rev. Lett. **70**, 694 (1993).

[36] G. van der Laan, Angular momentum sum rules for x-ray absorption, Phys. Rev. B **57**, 112 (1998).

[37] G. van der Laan, T. Hesjedal, and P. Bencok, Polarization analysis by means of individual soft x-ray absorption spectra of rare earths, Phys. Rev. B **106**, 214423 (2022).

[38] T. Mairoser, F. Loder, A. Melville, D. G. Schlom, and A. Schmehl, Influence of chemical doping on the magnetic properties of EuO, Phys. Rev. B **87**, 014416 (2013).

[39] T. Mairoser, A. Schmehl, A. Melville, T. Heeg, W. Zander, J. Schubert, D. E. Shai, E. J. Monkman, K. M. Shen, T. Z. Regier, D. G. Schlom, and J. Mannhart, Influence of the substrate temperature on the Curie temperature and charge carrier density of epitaxial Gd-doped EuO films, Appl. Phys. Lett. **98**, 102110 (2011).

[40] H. Miyazaki, H. J. Im, K. Terashima, S. Yagi, M. Kato, K. Soda, T. Ito, and S. Kimura, La-doped EuO: A rare earth ferromagnetic semiconductor with the highest Curie temperature, Appl. Phys. Lett. **96**, 232503 (2010).

[41] P. Liu, J. Tang, J. A. C. Santana, K. D. Belashchenko, and P. A. Dowben, Ce-doped EuO: Magnetic properties and the indirect band gap, J. Appl. Phys. **109**, 07C311 (2011).

[42] M. Takahashi, Origin of anomalous magnetization curve of electron-doped EuO, J. Phys. Soc. Jpn. **80**, 075001 (2011).

[43] M. Arnold and J. Kroha, Simultaneous ferromagnetic metal-semiconductor transition in electron-doped EuO, Phys. Rev. Lett. **100**, 046404 (2008).

[44] C. Haas, Magnetic semiconductors, CRC Crit. Rev. Solid State Sci. **1**, 47 (1970).

[45] H. Miyazaki, T. Ito, H. J. Im, S. Yagi, M. Kato, K. Soda, and S. Kimura, Direct observation of momentum-dependent exchange interaction in a Heisenberg ferromagnet, Phys. Rev. Lett. **102**, 227203 (2009).

[46] T. Stollenwerk and J. Kroha, Theory of Curie temperature enhancement in electron-doped EuO, Phys. Rev. B **92**, 205119 (2015).

[47] H. Rho, C. S. Snow, S. L. Cooper, Z. Fisk, A. Comment, and J.-Ph. Ansermet, Evolution of magnetic polarons and spin-carrier interactions through the metal-insulator transition in $Eu_{1-x}Gd_xO$, Phys. Rev. Lett. **88**, 127401 (2002).

[48] P. Liu and J. Tang, A magnetic polaron model for the enhanced Curie temperature of EuO_{1-x}, J. Phys.: Condens. Matter **25**, 125802 (2013).